Published in IEEE TRANSACTIONS ON ANTENNAS AND PROPAGATION, VOL. 70, NO. 11, NOVEMBER 2022

On the effect of grid orthogonalization in stability and accuracy of a FDTD Subgridding method

Antonio M. Valverde, Miguel R. Cabello, Clemente Cobos Sánchez, A. Rubio Bretones, and Salvador G. Garcia, *Senior Member, IEEE*

***Abstract*—We present a general-purpose subgridding inspired on a simplified Orthogonalized Integral-based method, leading to a simple and efficient algorithm with strong stability. It is based on a 2:1 transition ratio between coarse and finer zones and a natural local time stepping strategy to connect the domains. We provide a closed form for the stability condition and prove it heuristically, to show that roughly a 65% time-step reduction is enough to achieve stability. Results for coupling through lossy thin shells, compared to classical sub-cell impedance boundary methods, serve to prove the high accuracy of this method.**

***Index Terms*—Finite-difference time domain (FDTD), Subgridding, Electromagnetic compatibility (EMC), Shielding effectiveness (SE),**

I. Introduction

In the world of computational electromagnetic (CEM) algorithms, the finite-difference time-domain (FDTD) method [1] is known for being a simple yet powerful solution to solve Maxwell's equations in time domain. However, the explicit causal propagator requires to find the solution in a spatial mesh resolving both free-space and homogeneous regions of materials, as well as involved geometrical boundaries between them (curvatures, slots, etc.). This fact makes this method to require huge computational resources, since fine details dominate the global time and space steps that must be used for the whole simulation. A common approach is to employ some subcell algorithms taking into account the local physics: for instance, for lossy thin slabs a proper assumption is to assume waves propagating perpendicularly across the boundary [2]–[4], or for curved geometries a locally integral formulation, so-called conformal, can deal with smooth curvatures of metal and dielectric materials [5]–[7]. However, a more general solution is found by combining regions with different cell sizes and devising some algorithms to connect the solution between them. This gives rise to a family of techniques known as subgridding methods, and several approaches exist in literature [8]–[13].

Subgridding methods can be seen as a way to subdivide cells (coarse cells) into smaller subcells (fine cells), each one preserving the shape and orientation of the original, but having a smaller size. In most formulations, this division is applied recursively. The refinement ratio between the coarse and the fine cell sizes is usually an integer number to create the so-called conforming meshes. Each cell behaves like an usual Yee cell for every other neighbor one that shares the same size, implying that the complexity lies exclusively in the boundary between different levels. This becomes even more complex when each level has a different time-step according to its space-step, thus also requiring a local time stepping (LTS) strategy.

Despite being a promising field that could be potentially combined with any other subcell algorithms, subgridding methods typically present problems such as instabilities, spurious reflections and accuracy issues [14], [15]. Many different approaches have been made in order to solve these problems, such as extense overlapping boundaries for better interpolations, digital filters [14], [16]. However, to our best knowledge, a broadly accepted optimum solution has not been yet found.

In this paper, we present a detailed explanation and in-depth study of the Orthogonalized Integral-based Subgridding (OISG) approach presented in [10], [11]. The authors claimed the algorithm to be stable and accurate, relying in the fact that it removed the need for interpolations of non-existing field components in the integral formulation of Maxwell's equations, thus allowing the algorithm to meet a null-divergence property. Based on this, in this paper, we here carry out a further study of the algorithm itself, by varying what we call the orthogonalization parameter, proposing a stable LTS approach, and studying its overall stability and accuracy. To our best knowledge not so exhaustive description and analysis has been conducted elsewhere and it serves to prove the feasibility of this method.

The rest of the paper is organized as follows. In section II, we explain the fundamentals of the method, and how we can obtain simple equations in order to solve field components values in the subgridding interface using an integral formulation of Maxwell equations. In section III we explain the details related to the LTS methodology. Section IV obtains theoretical and simulation conditions for the stability of the method. In section V, we discuss the validity of the presented method using canonical EMC application of SE. Finally, we draw conclusions in section VI.

II. Method description

The subgridding method analyzed in this work is based on that of [10], and also relies in the division of every FDTD

The 1st 2nd, 4th and 5th authors are with the Dept. of Electromagnetism, University of Granada, Fuentenueva s/n, 18071 Granada. The 3th author are with the Dept. of Engineering of System and Electronic, University of Cadiz, Avenida de la Universidad, 10, E-11519, Puerto Real (Cádiz), Spain. Corresponding author e-mail: mcabello@ugr.es

This research was funded by: the Spanish Ministry of Science and Innovation (MICINN) under project eSAFE-UAV PID2019-106120RB-C32, and by the 2014-2020 ERDF Operational Programme and by the Department of Economy, Knowledge, Business and University of the Regional Government of Andalusia. Project reference: FEDER-UCA18-105867.

cell using a 1:2 refinement ratio, which is applied recursively, leading to different subgrid levels, each one containing cells with half the length of that of the next larger level (see Fig. 1); in 3D a cell at one level results thus divided into 8 ones at the level above. We will denote with $n_{\text{sg}} = 0$ the finest level, and each coarser level increases n_{sg} by one until the coarsest level N_{sg}. For simplicity, we will also assume an isotropic cubic lattice $\Delta x_{n_{\text{sg}}} = \Delta y_{n_{\text{sg}}} = \Delta z_{n_{\text{sg}}} \equiv \Delta_{n_{\text{sg}}}$ for any given level. The space-step at a given level fulfills,

$$\Delta_{n_{\text{sg}}} = 2^{n_{\text{sg}}} \Delta_0. \tag{1}$$

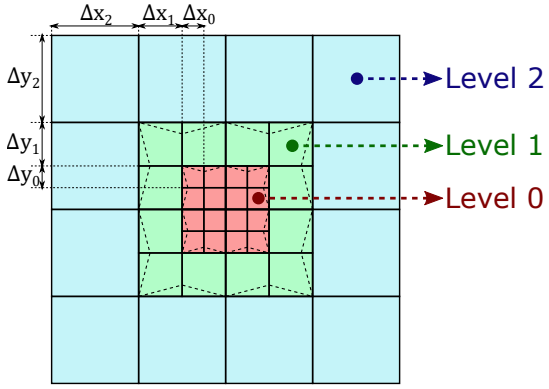

Fig. 1: Cross section of a subgridded region with a refinement ratio of 1:2. Each color represents cell at the same subgrid level.

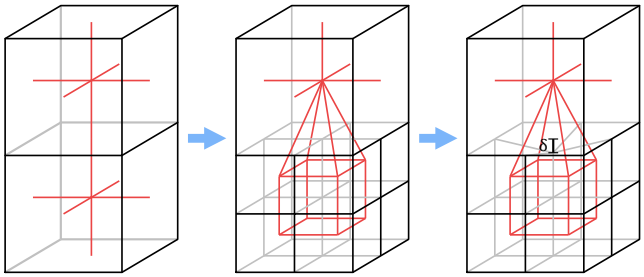

Fig. 2: Stages followed to construct the 3D subgridded mesh at the boundary. Black lines represent main (electric) grid and red lines represent dual (magnetic) grid.

We will refer to the set of all cells belonging to the same subgrid level as *domain-level*, and as *boundary-level* to the boundary surface lying between neighbor domain-levels. Continuing with the procedure of [10], we introduce a deformation of cells at the *boundary-level*, by moving the central vertex of the face of each coarse cell by a certain offset distance $\delta_{n_{\text{sg}}}$ inside the fine region (see Fig. 2). For simplicity, this offset is taken to be proportional to the finer cell size $\Delta_{n_{\text{sg}}}$ for each transition, thus keeping constant the ratio $\delta_r \equiv \delta_{n_{\text{sg}}}/\Delta_{n_{\text{sg}}}$ throughout all the transitions.

Locally, all cells inside of a domain-level are considered as part of a usual FDTD grid, meaning that the updating algorithm is the usual unmodified Yee one. However, the usual Yee algorithm cannot be used to update some of the fields in

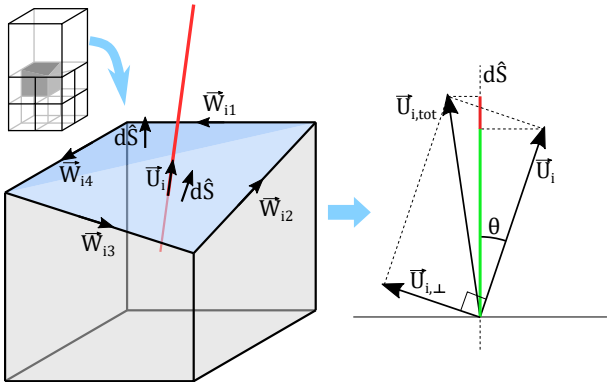

Fig. 3: Projection of a given field $\vec{U}$ on a direction perpendicular to a surface, where $d\hat{S}$ is a unit vector along a Cartesian direction, $\vec{U}_i$ is a known component, and $\vec{U}_{i,\perp}$ is an unknown component perpendicular to $\vec{U}_i$ contained in the surface defined by $\vec{U}_i$ and $d\hat{S}$. The green line is the known projection on the surface normal, and the red line is the unknown one.

the boundary-levels, and different approaches can be used in order to solve this issue [9], [12], [13], [17]. We will next describe the one chosen in this work which is based on [10]. For this, let us refer to the electric grid as the main grid, and to the magnetic grid as dual grid, where each one is defined by the edges along each component of the discrete EM field. Fig. 2 depicts how these grids behave at the boundary, and Fig. 3 shows the detail of one of the subgridded cells. We notice that the upper face of the cell is, in general, non planar. In that figure we have chosen two triangles forming a dihedral to account for this effect: one of them formed by the two Cartesian edges, and the other one formed by the *non-Cartesian* ones, though any other choice, even a smooth curved surface, could also be assumed. Hence, the integration surface, as well as the edges, do not necessarily have a pure Cartesian direction.

Let us consider an arbitrary known field component $\vec{U}_i$ that lies along some edge of either the main or the dual grid, and decompose it into $\vec{U}_{i,\text{tot}} = \vec{U}_i + \vec{U}_{i,\perp}$ (see, for example, Fig. 3). In the same way, let us consider a surface S whose contour are the edges at the dual field $\vec{W}$. Maxwell's curl equation in integral form for this field is:

$$\frac{d}{dt}\int_S \vec{U}\cdot d\vec{S} = \frac{1}{\{\varepsilon,\mu\}}\left(\pm\oint_{\partial S}\vec{W}\cdot d\vec{l} - \int_S \vec{J}\cdot d\vec{S}\right), \tag{2}$$

where $\vec{U}$ is $\vec{E}$ ($\vec{H}$), $\vec{W}$ is $\vec{H}$ ($\vec{E}$) and sign $\pm$ is positive (negative) if we are considering Ampere's Law (Faraday's Law). Since the field components $\vec{W}$ always lie along the edges of its own grid, the linear integral can be easily discretized as

$$\oint_{\partial S}\vec{W}\cdot d\vec{l} \simeq \sum_j W_{ij} l_{ij}, \tag{3}$$

where W_{ij} are the discrete field components around $\vec{U}_i$, and l_{ij} are the lengths of their corresponding grid edges. Note that

this sum might be over an arbitrary number of components, not necessarily four.

The surface integral, on the other hand, needs more analysis. If we approximate $\vec{U} = \vec{U}_{i,\text{tot}}$ to be constant over the surface, we may decompose it as follows

$$\begin{aligned}\int_S \vec{U}\cdot d\vec{S} &= \int_S \vec{U}_i \cdot d\vec{S} + \int_S \vec{U}_{i,\perp}\cdot d\vec{S} \\ &\simeq U_i \int_S \hat{U}_i \cdot d\vec{S} + U_{i,\perp}\int_S \hat{U}_{i,\perp}\cdot d\vec{S} = \\ &= S_{\text{eq},i}\, U_i + S_{\text{eq},i,\perp}\, U_{i,\perp},\end{aligned} \tag{4}$$

where we have defined $S_{\text{eq},i}$ and $S_{\text{eq},i,\perp}$ as the *equivalent surfaces* for each field component. These have the following expressions:

$$\begin{aligned}S_{\text{eq},i} &= \sum_j S_j \cos\theta_{ij}, \\ S_{\text{eq},i,\perp} &= \sum_j S_j \sin\theta_{ij},\end{aligned} \tag{5}$$

where we assumed that the surface can be split in a number of planar surfaces S_j (for example, the two triangles of Fig. 3), and θ_{ij} are the angles between the component $\vec{U}_i$ and the surface normal vectors. It should be noted that Stokes' theorem grants us that any surface in Eq. 5 will lead to the same result, as long as its contour is formed by the surrounding edges.

Since $U_{i,\perp}$ is unknown, in order to avoid interpolations, we will make a reasonable assumption: the contribution to the surface integral of the perpendicular component will be neglected, so that: $S_{\text{eq},i}U_i \gg S_{\text{eq},i,\perp}U_{i,\perp}$ and consequently we assume,

$$\int_S \vec{U}\cdot d\vec{S} \simeq S_{\text{eq},i}U_i. \tag{6}$$

In order to reduce the effect of this assumption, it will be desirable to minimize $\sin\theta_{ij}$, which is the goal of the orthogonalization method introduced in [10], [11]. This allows us to modify some grid vertices by a parameter δ (see Fig. 2) and therefore, for some integration surfaces, enforce the angles $\theta_{ij} = 0$, and thus $\sin\theta_{ij} = 0$ as well (see Fig. 2 and Fig. 3), which justifies Eq. 6.

The explicit updating algorithm is found by replacing by centered finite-difference the time derivative in Eq. 2 with a given time-step $\Delta t_{n_{\text{sg}}}$ to yield in general for any field component U_i:

$$\begin{aligned}U_i|^{n+1} &= C_{0,i}\ U_i|^n \\ &+ \frac{C_{1,i}}{S_{\text{eq},i}}\sum_j l_{i,j}\ W_{i,j}|^{n+1/2} \\ &+ C_{2,i}\ J_i|^{n+1/2}\end{aligned} \tag{7}$$

where $C_{0,i}$, $C_{1,i}$ and $C_{2,i}$ are constants depending on media and the time-step. Note, that this step may be the same or desirable differ for each level n_{sg} to take profit of the stability condition in a piecewise manner, with the constraints due to the boundary equations, as will be discussed in Sec. III.

Equation (7) gives us an easy way to classify every non-trivial discrete field component near the boundary-levels based on their equivalent surfaces and their edge length. For a cubic lattice, we can identify 6 types for the E-field, and 4 types for the H-field components. This classification is shown in Tab. I and Fig. 4.

TABLE I: Field types classification for boundary-levels. In every expression, Δ refers to the cell length of the fine level in the considered .

Electric		
Type	S_{eq}/Δ^2	l/Δ
1	$\frac{3+\delta_r}{4\sqrt{1+\delta_r^2}}$	$\sqrt{1+\delta_r^2}$
2	9/4	1
3	1	$1-\delta_r$
4	3	1
5	2	1
6	3/2	1

Magnetic		
Type	S_{eq}/Δ^2	l/Δ
1	$\frac{3+\delta_r}{\sqrt{11}}$	$\frac{\sqrt{11}}{2}$
2	$1-\frac{\delta_r}{2}$	1
3	$1-\delta_r$	1
4	N/A At the finest level this parameter makes no sense	2

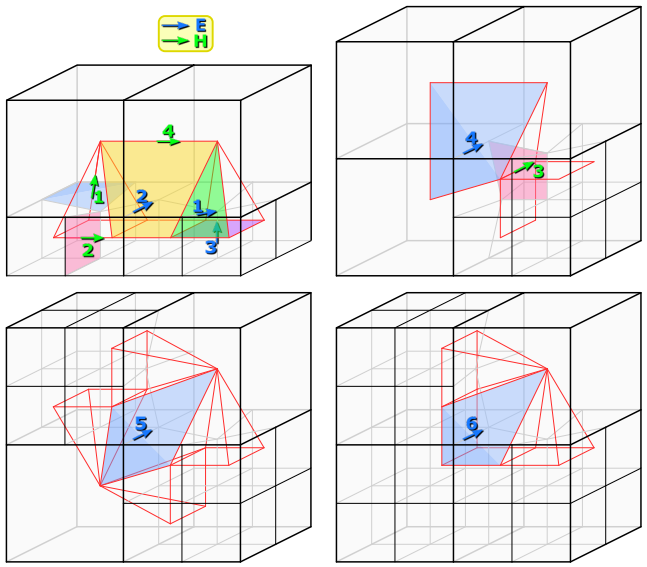

Fig. 4: Subgridding *boundary-level* field types. Each field type is classified and their integration surfaces are represented. The number of each field type correspond to Tab. I.

III. Local time stepping

The time-step for each subgrid level $\Delta t_{n_{\text{sg}}}$ is a topic that needs a thorough analysis. Let us consider a given mesh with maximum grid level N_{sg}. First, let us assume that we use the same time steps for all subgriding level, $\Delta t_{n_{\text{sg}}} = \Delta t$. Here, in order to apply the Courant–Friedrichs–Lewy stability (CFLN) condition [18] [19], we need to define the CFLN number. As we have different subgrid levels, it will depend on each level as follows:

$$\text{CFLN}_{n_{\text{sg}}} = \frac{\sqrt{3}\, c_0\, \Delta t_{n_{\text{sg}}}}{\Delta_{n_{\text{sg}}}}. \tag{8}$$

Now, by using the fact that the time-step is constant and Eq. 1 we obtain that

$$\mathrm{CFLN}_{N_{\mathrm{sg}}} = 2^{-N_{\mathrm{sg}}}\mathrm{CFLN}_0. \tag{9}$$

The stability condition requires that $\mathrm{CFLN}_{n_{\mathrm{sg}}} \leqslant 1\ \forall n_{\mathrm{sg}}$, which forces

$$\mathrm{CFLN}_{N_{\mathrm{sg}}} \leqslant 2^{-N_{\mathrm{sg}}}. \tag{10}$$

Though no special algorithm is then required to connect regions with different grid sizes, this minimum time step is a severe constraint since it oversamples the coarser level unnecessarily, drastically decreasing the computational efficiency. Additionally, increased CFLN implies increased phase dispersion errors in the coarse zones, which is a numerical phenomenon inherent to FDTD method. The reason for that, is that the numerical propagation velocity is not linear [18], [20], and it is different for each spectral component of the signal, and, in general, different from the actual speed of light. Only in one dimension, there is a *magic* CFLN not leading to dispersion errors.

Hence, let us consider the use of different time-steps for each level and describe the connection between the time-stepping procedures at the boundaries. Particularly, in order to obtain the same CFLN number at every level, the choice of the time-step must comply with

$$\Delta t_{n_{\mathrm{sg}}} = 2^{n_{\mathrm{sg}}}\Delta t_0 \tag{11}$$

In this case, it is possible to use a CFLN value closer to 1 in the whole domain. The stability criterion however leads to a CFLN smaller than 1, as is further discussed in Sec. IV. The fact that every level has a different time-step means that it is necessary to coordinate the update of each grid in the boundary-levels. For this purpose, let us consider an arbitrary boundary-level and focus on the discrete field components that, when updated, use another one that belongs to a different subgrid level. If we look at Fig. 4, we may see that the affected fields in the fine level are only electric (types 2, 4, 5, 6) and that the affected ones in the coarse level are only magnetic (type 4). This means that it is only necessary to find a scheme that explains how to use fine electric components to update coarse magnetic ones and vice versa. The LTS scheme we have implemented is illustrated in Fig. 5 and it works as follows:

- For each electric or magnetic coarse component, we consider simultaneous electric fine ones existing as well.
- Each coarse magnetic field component is updated with the immediate previous fine electric component, which is correctly time-placed.
- If a fine electric component is simultaneous with a coarse electric one, it will use the immediate previous coarse magnetic component, which is not correctly time-placed.
- If a fine electric component is simultaneous to a coarse magnetic one, it will use its simultaneous coarse magnetic component.

We must note that, for the local time stepping used by the subgridding method, it is necessary to *extend* the temporal location for several components. That is, each electric component located in a subgridding boundary, alternates the use of a delayed and an over-advanced magnetic components in their update. This cannot be solved in a flawless manner, and it becomes an intrinsic characteristic of this method.

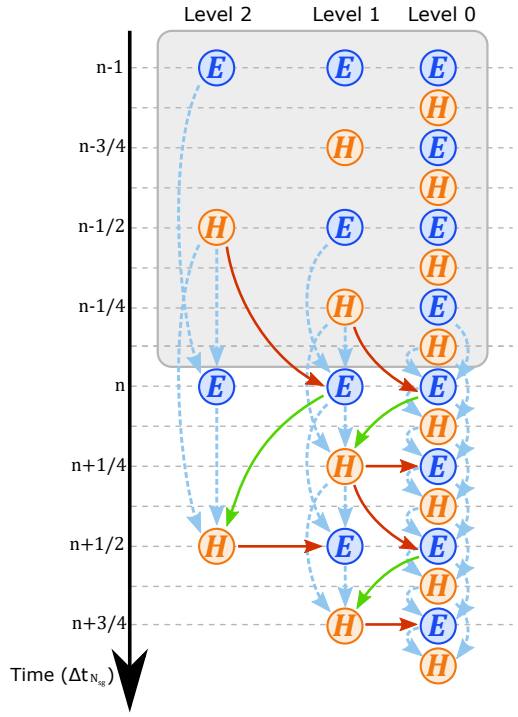

Fig. 5: Temporal update scheme for the subgridding local time stepping implementation. For every field update (electric and magnetic) in a certain domain-level, we recursively update the electric and then the magnetic field components in the next finer level. Blue dashed arrows show intralevel field components usage (usual FDTD); green arrows show usage of electric fine components to update magnetic coarse ones; red arrows show usage of magnetic coarse components to update electric fine ones.

IV. Stability Analysis

As expected, the stability is degraded away from the usual one due to the algorithm used at the subgridding boundaries (see Fig. 4). In this section, we study the maximum CFLN value that we may use for each possible value of δ/Δ. For this purpose we provide two different approaches. First, a sort of theoretical one based on the integration surfaces and lines of the algorithm [7], [21]; second, an heuristic study using real simulations. We must note that, using the results obtained in this section, we have simulated lots of different cases for over 10^7 iterations and the algorithm has proved stable in all of them.

A. Analytical condition

In this section, a sufficient condition is derived of the interaction of neighbour electric and magnetic fields. First, let us write the general update equation for the FDTD method without external sources.

$$U_i|^{n+1} = G_{0,i}\ U_i|^n + G_{1,i} \sum_j \mathrm{sgn}_{i,j}\, l_{i,j}\ W_{i,j}|^{n+1/2} \tag{12}$$

where $\mathrm{sgn}_{i,j} = \pm 1$ depends on the relative orientation of the fields. We note that this general equation applies for both the usual FDTD method and the subgridding algorithm in a boundary-level (eq. Eq. 7), where

$$G_{0,i} = C_{0,i},$$
$$G_{1,i} = \frac{C_{1,i}}{S_{\mathrm{eq},i}}. \tag{13}$$

Let us consider the update equation of a given electric component E_i in vacuum using

SGG: xxx???

, but focusing only on one of its magnetic neighbor components H_j. In this case we have

$$E_i|^{n+1} = E_i|^{n} + \mathrm{sgn}_{i,j}\, G_{1,i}\, l_j\, H_j|^{n+1/2} + [...]. \tag{14}$$

Now, if we consider the previous update equation of the component $H_j|^{n+1/2}$ and substitute it in Eq. 14, we obtain

$$E_i|^{n+1} = (1 - \mathrm{Acc}_{i,j})\, E_i|^{n} + [...]. \tag{15}$$

where

$$\mathrm{Acc}_{i,j} = G_{1,i}\, G_{1,j}\, l_i\, l_j \tag{16}$$

is the coupled update constants of the given neighbor field components. We note that the product $\mathrm{sgn}_{i,j}\mathrm{sgn}_{j,i} = -1$.

Here, we may particularize for the trivial case in free-space with a cubic lattice,

$$\mathrm{Acc}_{i,j} = \frac{(\Delta t)^2}{\varepsilon_0 \mu_0 \Delta^2} = \frac{\mathrm{CFLN}^2}{3}, \tag{17}$$

and also for the subgridding algorithm in a boundary-level,

$$\mathrm{Acc}_{i,j} = \frac{(\Delta t)^2\, l_i l_j}{\varepsilon_0 \mu_0 S_{\mathrm{eq},i} S_{\mathrm{eq},j}} = \frac{\mathrm{CFLN}^2}{3} \left(\frac{S_{\mathrm{eq},i}}{l_i \Delta} \frac{S_{\mathrm{eq},j}}{l_j \Delta} \right). \tag{18}$$

For the first case, the Courant criterion stablishes the condition $\mathrm{CFLN} < 1$, which leads us to

$$\mathrm{Acc}_{i,j} < 1/3. \tag{19}$$

As the update equation for the subgridding boundary-level is analogous to the FDTD method, we consider it a suitable approach to transfer the condition obtained in Eq. 19. Now, we must note that this condition applies to all the possible combination of neighbor field components, which leads us to

$$\mathrm{CFLN} \leqslant \min_{(i,j)\mathrm{neighbours}} \sqrt{\frac{S_{\mathrm{eq},i}}{l_i \Delta} \frac{S_{\mathrm{eq},j}}{l_j \Delta}}. \tag{20}$$

Note that the deformation parameter δ has a strong effect in the stability condition, as the equivalent surfaces and integration lines depend on it. We must also point out that the LTS described in Fig. 5 is the only one up to our experience to provide stable results with this criterion, and no instabilities have been appreciated in a large number of complex test-cases simulated for long time in low-frequency slowly converging situations. Any other time LTS scheme to connect fine and coarse meshes, has proven to our best knowledge, to lead to unstable schemes. Further analytical studies are ongoing and they are the subject of a future paper.

B. Heuristic approach

In this section, we aim to obtain an approximation for the stability of the method by running many simulations using different values of δ_r and CFLN. We have varied δ_r in the interval $[0, 1]$, and for each value we have found the highest CFLN for which the simulation has been stable after $t = 10^7 \Delta t_{\mathrm{coarse}}$. In every simulation, the coarse subgrid level used is $N_{\mathrm{sg}} = 2$.

For these simulations, we have used a case without materials and with a random distribution of fine cells, making sure that all the field types defined in Tab. I appear. An example of a minimal case containing all field types may be seen in Fig. 6.

The results obtained by both approaches are shown in Fig. 7. It can be seen that the maximum value of CFLN in both cases is obtained around $\delta_r = 1/3$, with $\mathrm{CFLN}_{\mathrm{max}} \simeq 0.67$.

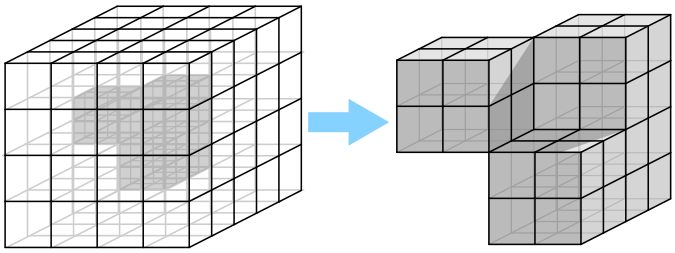

Fig. 6: Scheme of a minimal simulation containing all field types from Tab. I.

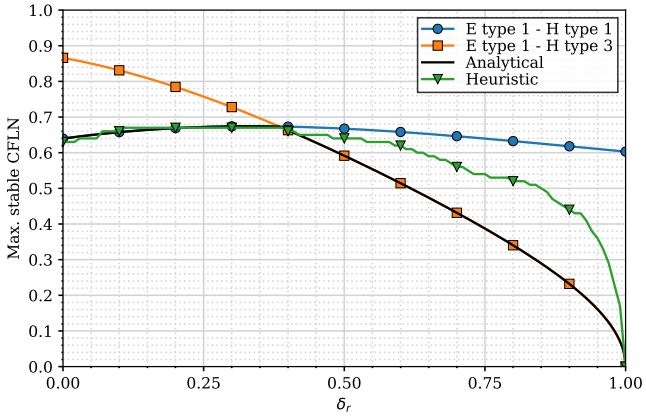

Fig. 7: Maximum stable CFLN value as a function of δ_r.

V. Numerical Results

The accuracy and efficiency of the subgridding algorithm described above has been assessed by using a challenging resonant test-case based on spherical conductive shell with 20 mm of thickness and 1 m of medium radius, and an electric conductivity of 5 S/m. The sphere is illuminated with a plane-wave tilted $45°$ with respect to the x axis. The plane-wave is excited with a Gaussian pulse with -3 dB decay in amplitude at 1 GHz ($f(t) = e^{-(t-t_0)^2/w^2}$, $t_0 = 0.696$ ns, $w = 0.187$ ns.). The computational volume is truncated by convolutional PMLs.

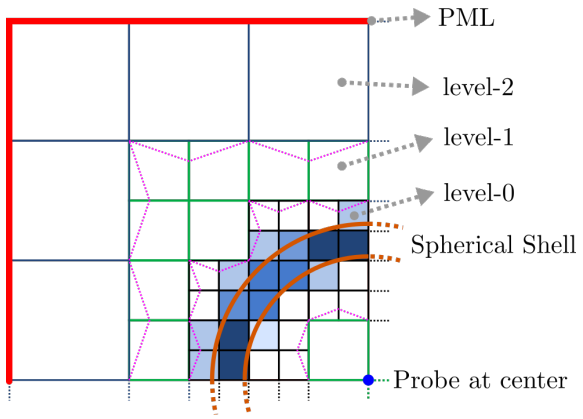

Fig. 8: 2D cross-section of the spherical shell test case. In blue the cells affected by the conductive shell, the rest of the cells in white. The dotted purple lines represent the warped transition between two adjacent grid levels.

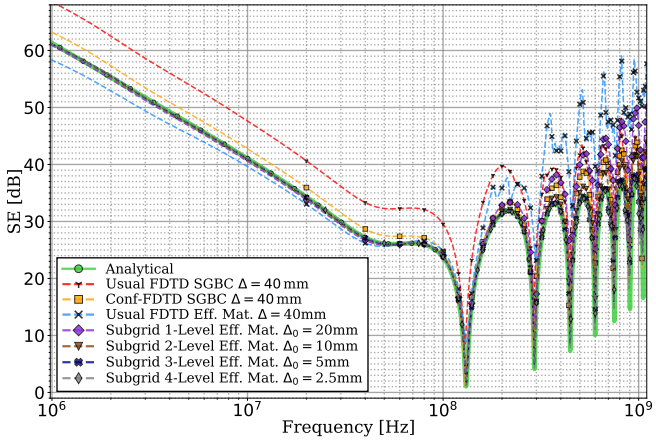

Fig. 9: E-field at the center of the sphere. The shielding effectiveness SE (inverse of the transfer function) has been used as the figure-of-merit defined as $\mathrm{SE} = 20\log\left(|E_{\text{incident}}|/|E_{\text{center}}|\right)$.

In Fig. 9, we show the result obtained with the proposed subgridding technique. The finest grid region is generated so that the spherical shell lays wholly inside the finest level. The size of the coarsest grid size remains fixed at 40 mm. We compare results obtained with different finest resolutions $\{20, 10, 5, 2.5\}$ mm corresponding to a number of subgrid levels of $\{1, 2, 3, 4\}$ respectively in Fig. 8. The LTS technique proposed in sec.III, yields a global $\mathrm{CFLN}_{n_{\text{sg}}}$ of 0.67 corresponding to $\delta_r = 1/3$ fig. 7.

The spherical shell has been modeled as a volume in the finest grid region. The constitutive parameters for the conductivity associated to a cell that are partially inside of the spherical shell volume, is evaluated by using effective average parameters method based on [22],

$$\sigma_{\text{eff}}\left(i,j,k\right) = \sigma_{\text{shell}}\frac{V_{\text{partial}}\left(i,j,k\right)}{V_{\text{cell}}\left(i,j,k\right)}$$

where σ_{eff} is the conductivity of a partially filled cell. V_{cell} is the volume of a cell; for instance for a cubic cell in the finest grid $V_{\text{cell}} = \left(\Delta_{\text{finest}}\right)^3$, and V_{partial} is just the partial volume of a cell inside of the spherical shell. The rest of the space and grid levels not traversed by the spherical shell is simply free-space.

In Fig. 9, we have also included, for reference, results found with the SGBC method of [2], [23], which is a specific sub-cell model to deal with conductive thin panels, both for staircased meshes, and for conformal meshes [24]. Both have been simulated with a 40 mm of cell size and 5 mm of 1D-cell size in the thin-panel. For the staircase mesh, we used a CFLN of 0.9, and for the conformal one [5] we use a CFLN of 0.7, corresponding with a relaxed factor of 0.33 [7]. The results with the aforementioned methods are compared to closed-form analytical data found from [25].

The effect of tree different degree of deformation $\delta_r = \{0, 0.33, 0.5\}$ has been tested using the same spherical test with $\Delta_0 = 10$ mm and $N_{\text{sg}} = 2$, the time step used have been chosen in accordance with Fig. 7. The results are shown in Fig. 10 and no changes in accuracy have been appreciated.

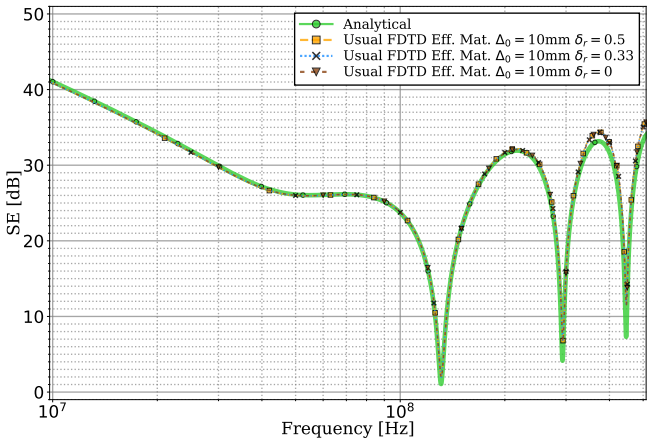

Fig. 10: SE for different degree of deformation.

In view of the results, the proposed subgridding method show a high accuracy, in comparison with the thin-panel method [3], [23]. As shown in [26], methods for thin panels exhibit a typical offset error of about, 6 dB for staircased meshes (reducing up to 1-2 dB for conformal). This error appears because thin panel techniques assume plane-wave propagation inside the thin panel, along the direction normal to its surface, which is a reasonable hypothesis only for highly conductive media [2]. The error is still higher for structured mesh due to inherent ambiguity of the surface normal on staircased edges, when curved surfaces are approximated by a structured mesh.

Table II shows the computational resources of the simulation. Note that the test-case proposed in this article is a case where the SGBC methods are already computationally very efficient. In this sense, subgridding methods are not competitive in accuracy with respect to subcell specific techniques such as SGBC. However, SGBC assumes a TEM propagation condition inside the pannel [2], which does not hold for low conductivities. Obviously, the generality of subgridding methods do not require to make this assumption, and naturally present a high-precision.

TABLE II: Efficiency results

Method	CFLN	Δ_{min} [mm]	Δ_{max} [mm]	CPU Gain	Memory Gain
FDTD N_{sg}=1	0.67	20	40	2.8	1.6
FDTD N_{sg}=2	0.67	10	40	5.1	3.1
FDTD N_{sg}=3	0.67	5	40	7.9	5.2
FDTD N_{sg}=4	0.67	2.5	40	11.5	8.4

VI. Conclusions

In this paper, we have presented a complete description of the orthogonalization effects on the stability and accuracy of the subgridding method proposed in [10], [11]. This ortogonalization consists in a deformation of the cells at the transition between neighbors subgrid levels in order to get a reciprocal algorithm and avoid interpolations. This deformation implies a new distribution of electric and magnetic fields at the deformation region, which would no longer be associated with a usual FDTD grid, and, in turn, a more complex updating equation than the Yee's method is yielded. In the first part of the paper, we have explained the subgridding method showing all details about its updating equations. Also we introduce the a local time stepping technique to increase the stability limit, and, consequently, the method efficiency. In the second part of the paper, we have developed a method to obtain the optimal orthogonalization parameter for the best CFLN. Ultimately, the method has been validated by using a shielding problem. In view of the results, this subgridding method is a computationally very efficient, high accurate, and flexible way to address general multi-scale problems in FDTD.

Acknowledgments

The work described in this paper has received funding from the Spanish MICINN, EU FEDER under Project PID2019-106120RB-C33 and from Airbus through the Alhambra-LFT LOU art. 33 contract.

References

[1] K. Yee, "Numerical solution of initial boundary value problems involving Maxwell's equations in isotropic media," IEEE Transactions on Antennas and Propagation, vol. 14, no. 3, pp. 302–307, May 1966.

[2] M. R. Cabello, L. D. Angulo, J. Alvarez, I. Flintoft, S. Bourke, J. Dawson, R. G. Martin, and S. G. Garcia, "A hybrid crank-nicolson fdtd subgridding boundary condition for lossy thin-layer modeling," IEEE Transactions on Microwave Theory and Techniques, 2017, accepted.

[3] M. Sarto, "A new model for the FDTD analysis of the shielding performances of thin composite structures," Electromagnetic Compatibility, IEEE Transactions on, vol. 41, no. 4, pp. 298 –306, Nov. 1999.

[4] I. D. Flintoft, J. F. Dawson, L. Dawson, A. C. Marvin, J. Alvarez, and S. G. Garcia, "A modular test-suite for the validation and verification of electromagnetic solvers in electromagnetic compatibility applications," IEEE Transactions on Electromagnetic Compatibility, vol. 59, no. 1, pp. 111–118, Feb. 2017.

[5] S. Dey and R. Mittra, "A locally conformal finite-difference time-domain (FDTD) algorithm for modeling three-dimensional perfectly conducting objects," Microwave and Guided Wave Letters, IEEE, vol. 7, no. 9, pp. 273–275, September 1997. [Online]. Available: http://ieeexplore.ieee.org/stamp/stamp.jsp?tp=&arnumber=622536

[6] N. Kaneda, B. Houshmand, and T. Itoh, "FDTD analysis of dielectric resonators with curved surfaces," IEEE Transactions on Microwave Theory and Techniques, vol. 45, no. 9, pp. 1645–1649, Sep. 1997.

[7] M. R. Cabello, L. D. Angulo, J. Alvarez, A. R. Bretones, G. G. Gutierrez, and S. G. Garcia, "A new efficient and stable 3D conformal FDTD," IEEE Microwave and Wireless Components Letters, vol. 26, no. 8, pp. 553–555, Aug 2016.

[8] I. Kim and W. Hoefer, "A local mesh refinement algorithm for the time domain-finite difference method using maxwell's curl equations," IEEE Transactions on Microwave Theory and Techniques, vol. 38, no. 6, pp. 812–815, 1990.

[9] P. Thoma and T. Weiland, "A consistent subgridding scheme for the Finite Difference Time Domain method," International Journal of Numerical Modelling: Electronic Networks, Devices and Fields, vol. 9, no. 5, pp. 359–374, 1996. [Online]. Available: https://onlinelibrary.wiley.com/doi/abs/10.1002/%28SICI%291099-1204%28199609%299%3A5%3C359%3A%3AAID-JNM245%3E3.0.CO%3B2-A

[10] J. Ritter and F. Arndt, "A generalized 3d subgrid technique for the finite-difference time domain method," in Microwave Symposium Digest, 1997., IEEE MTT-S International, vol. 3, June 1997, pp. 1563–1566 vol.3.

[11] F. Arndt and J. Ritter, "Advanced fd-td techniques for the cad of 3d microwave components," Electromagnetics, vol. 23, no. 2, pp. 153–168, 2003. [Online]. Available: https://doi.org/10.1080/02726340390159487

[12] K. Xiao, D. J. Pommerenke, and J. L. Drewniak, "A three-dimensional fdtd subgridding method with separate spatial and temporal subgridding interfaces," in Electromagnetic Compatibility, 2005. EMC 2005. 2005 International Symposium on, vol. 2. IEEE, 2005, pp. 578–583.

[13] J.-P. Bérenger, "The huygens subgridding for the numerical solution of the maxwell equations," Journal of Computational Physics, vol. 230, no. 14, pp. 5635–5659, 2011. [Online]. Available: https://www.sciencedirect.com/science/article/pii/S0021999111002075

[14] M. Celuch-Marcysiak and J. Rudnicki, "A study of numerical reflections caused by fdtd mesh refinements in 1d and 2d," in 15th International Conference on Microwaves, Radar and Wireless Communications (IEEE Cat. No.04EX824), vol. 2, 2004, pp. 626–629 Vol.2.

[15] B. Donderici and F. Teixeira, "Improved fdtd subgridding algorithms via digital filtering and domain overriding," IEEE Transactions on Antennas and Propagation, vol. 53, no. 9, pp. 2938–2951, 2005.

[16] C. Chang and C. D. Sarris, "A spatially filtered finite-difference time-domain scheme with controllable stability beyond the cfl limit: Theory and applications," IEEE Transactions on Microwave Theory and Techniques, vol. 61, no. 1, pp. 351–359, 2013.

[17] P. Chow, T. Kubota, and T. Namiki, "A stable fdtd subgridding method for both spatial and temporal spaces," in 2008 IEEE Antennas and Propagation Society International Symposium, 2008, pp. 1–4.

[18] A. Taflove, Computational Electrodynamics: The Finite-Difference Time-Domain Method. Boston: Artech House, 1995.

[19] R. Courant, K. Friedrichs, and H. Lewy, "On the partial difference equations of mathematical physics," IBM J. Res. Dev., vol. 11, pp. 215–234, March 1967. [Online]. Available: http://dx.doi.org/10.1147/rd.112.0215

[20] J. B. Schneider and C. L. Wagner, "Fdtd dispersion revisited: Faster-than-light propagation," IEEE Microwave and Guided Wave Letters, vol. 9, no. 2, pp. 54–56, 1999.

[21] S. Benkler, N. Chavannes, and N. Kuster, "A new 3-D conformal PEC FDTD scheme with user-defined geometric precision and derived stability criterion," Antennas and Propagation, IEEE Transactions on, vol. 54, no. 6, pp. 1843–1849, June 2006.

[22] S. Dey and R. Mittra, "A conformal finite-difference time-domain technique for modeling cylindrical dielectric resonators," IEEE Transactions on Microwave Theory and Techniques, vol. 47, no. 9, pp. 1737–1739, Sep. 1999.

[23] M. Cabello, L. Angulo, A. Bretones, R. Martin, S. Garcia, and J. Alvarez, "A new fdtd subgridding boundary condition for fdtd subcell lossy thin-layer modeling," in Antennas and Propagation (APSURSI), 2016 IEEE International Symposium on. IEEE, 2016, pp. 2031–2032.

[24] M. R. Cabello, L. D. Angulo, J. Alvarez, A. R. Bretones, and S. G. Garcia, "A new conformal fdtd for lossy thin panels," IEEE Transactions on Antennas and Propagation, vol. 67, no. 12, pp. 7433–7439, 2019.

[25] M. Ansarizadeh, "Calculation of ohe shielding effectiveness of carbon-fiber composite structures," Ph.D. dissertation, The Department of Electrical and Computer Engineering, Montreal, Quebec, Canada, September 2013.

[26] I. D. Flintoft, S. A. Bourke, J. F. Dawson, J. Alvarez, M. R. Cabello, M. P. Robinson, and S. G. Garcia, "Face-centered anisotropic

surface impedance boundary conditions in fdtd," IEEE Transactions on Microwave Theory and Techniques, vol. 66, no. 2, pp. 643–650, 2018.